Volume 11
Number 1
7 January 2021
Pages 1–360

Catalysis Science & Technology

rsc.li/catalysis

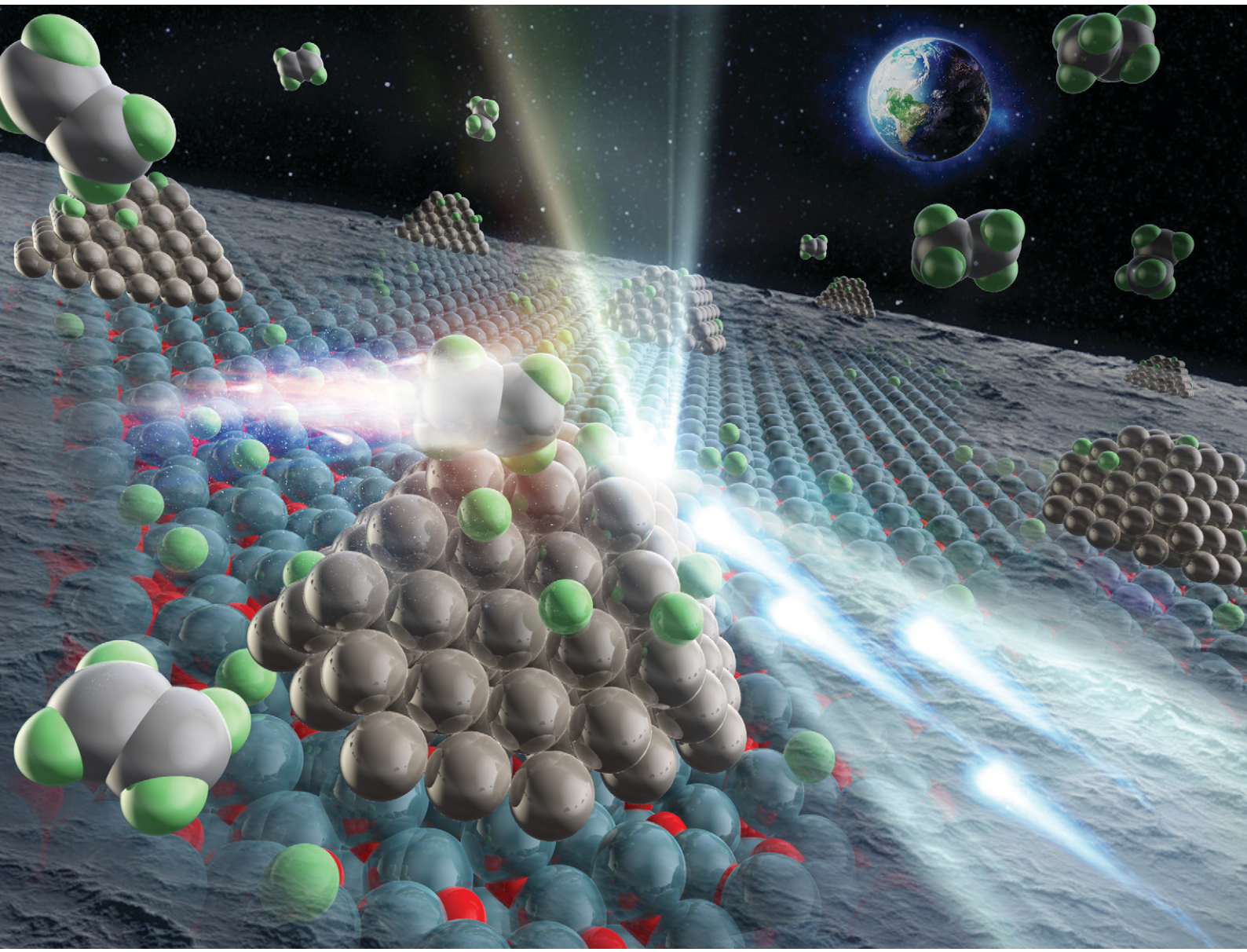

ISSN 2044-4761

ROYAL SOCIETY OF CHEMISTRY

PAPER

Hisao Yoshida, Tsunehiro Tanaka *et al.*
Identification of hydrogen species on Pt/Al_2O_3 by *in situ* inelastic neutron scattering and their reactivity with ethylene

Catalysis Science & Technology

ROYAL SOCIETY OF CHEMISTRY

PAPER

View Article Online
View Journal | View Issue

Cite this: *Catal. Sci. Technol.*, 2021, **11**, 116

Identification of hydrogen species on Pt/Al_2O_3 by *in situ* inelastic neutron scattering and their reactivity with ethylene†

Seiji Yamazoe, [ab] Akira Yamamoto, [ac] Saburo Hosokawa, [ad] Ryoichi Fukuda, [a] Kenji Hara, [e] Mitsutaka Nakamura, [f] Kazuya Kamazawa, [g] Tatsuya Tsukuda, [ah] Hisao Yoshida *[ac] and Tsunehiro Tanaka *[ad]

Received 9th October 2020,
Accepted 2nd November 2020

DOI: 10.1039/d0cy01968b

rsc.li/catalysis

Hydrogen (H) species adsorbed on catalyst surfaces are key intermediates in catalytic hydrogenation reactions over supported metal catalysts. However, individual identification of H species on the metal catalysts has not been established to date. Here, we elucidated the H species on Pt/Al_2O_3 by the combination of *in situ* inelastic neutron scattering (INS) and density functional theory (DFT). Several H species in the presence of H_2 were successfully identified at different sites on the Pt surface and Al_2O_3 support. The *in situ* INS and FT-IR measurements revealed that the hydride/atop Pt–H, bridged perimeter/terrace Pt–H–Pt, and threefold Pt_3–H are active intermediates in the C_2H_4 hydrogenation reaction, whereas the edge Pt–H–Pt is a rather inert species. In addition, the *in situ* measurements indicate that the Al_2O_3 itself acts as hydrogen storage material by mediating AlO–H and Al–H–Al species, which serve H species in the C_2H_4 hydrogenation reaction.

Introduction

Hydrogen (H) species is crucial intermediates in hydrogenation and reduction reactions in chemical synthesis and environmental chemistry.[1–6] In fine chemical synthesis, the selective hydrogenation reactions of functional groups such as $-NO_2$, –C═C–, –C≡C–, –C═O and –C≡N require the use of H_2 molecules to afford corresponding amines, alkanes, alkenes, alcohols and amines, respectively, which are essential for the chemical industry.[3–8] Supported metal catalysts are among the most promising candidates for selective hydrogenation reactions in practical applications because they are active, easily separated from products and reusable. The catalytic activity and selectivity of supported metal catalysts are dependent on the size, composition, geometric structure, surface coordination environment of the metal particles and also the properties of the support, which affect the electronic structure of the metals and provide the sites available for absorption and reaction in many cases. These structural factors induce a variety of structures and reactivity of the H species. One typical mechanism for the formation of the active H species proceeds by the homolytic dissociation of H_2 on metals such as Pt, Pd and Rh. The occupied d-orbitals of these metals donate their electrons to the antibonding orbital of H_2 to weaken the H–H bond.[9–12] In some cases, the H species migrate from the metal surface to the surface of support material, where the adsorbed substrates can be hydrogenated.[13–15] Another mechanism for the formation of the active H species proceeds by heterolytic dissociation of H_2 into H^+ and H^- species, which preferentially react with polar functional groups rather than nonpolar ones, typically at the interface between metal particles and metal oxide supports.[16] Thus, it is essential to elucidate both the adsorbed state and the dynamics of H species for the research and development of hydrogenation reactions.

The activation of H_2 and the dynamics of H species on the metal particles supported on metal oxide have been studied to understand the role of metals and supports during various hydrogenation reactions. Zaera reported that H_2 adsorption

[a] *Elements Strategy Initiative for Catalysts & Batteries (ESICB), Kyoto University, 1-30 Goryo-Ohara, Nishikyo-ku, Kyoto 615-8245, Japan*
[b] *Department of Chemistry, Graduate School of Science, Tokyo Metropolitan University, 1-1, Minami-osawa, Hachioji, Tokyo 192-0397, Japan*
[c] *Department of Interdisciplinary Environment, Graduate School of Human and Environmental Studies, Kyoto University, Yoshida-nihonmatsu-cho, Sakyo-ku, Kyoto 606-8501, Japan. E-mail: yoshida.hisao.2a@kyoto-u.ac.jp*
[d] *Department of Molecular Engineering, Graduate School of Engineering, Kyoto University, Kyotodaigaku Katsura, Nishikyo-ku, Kyoto 615-8510, Japan*
[e] *Department of Applied Chemistry, School of Engineering, Tokyo University of Technology, 1404-1 Katakura, Hachioji, Tokyo 060-0810, Japan*
[f] *Materials and Life Science Division, J-PARC Center, Japan Atomic Energy Agency, Tokai, Ibaraki 319-1195, Japan*
[g] *CROSS Neutron Science and Technology Center, Tokai, Ibaraki 319-1106, Japan*
[h] *Department of Chemistry, Graduate School of Science, The University of Tokyo, 7-3-1 Hongo, Bunkyo-ku, Tokyo 113-0033, Japan*

† Electronic supplementary information (ESI) available: Including XRD, XAFS, INS, DFT data, and activation mechanism. See DOI: 10.1039/d0cy01968b

(activation) on the Pt surface is the rate-determining step for the ethylene hydrogenation reaction.[5] High activity and selectivity in the hydrogenation of acetylene to ethylene were achieved by promoting the activation of H_2 and anticoking, which were induced by Pd catalysts.[17] In the case of the de-NO_x reaction with H_2 on Pt/MgO and Pt/CeO_2 catalysts, the H species activated by the Pt metal was found to migrate to the MgO and CeO_2 supports and react with the NO species adsorbed on these supports.[18] The H spillover on metal oxides well depends on the surface properties of the metal oxide supports, which may change during the hydrogenation reactions.[5,15] However, these reaction mechanisms have been based on the reaction results and structural characterization, but not yet supported by direct observation of the H species involved.

Inelastic neutron scattering (INS) spectroscopy is a powerful technique to investigate the H species adsorbed on the supported metal catalysts because of the extremely large cross section of neutron from ^{1}H.[19] INS spectroscopy is advantageous for analysing low-frequency vibration modes, such as vibration modes of functional groups containing H atom,[20,21] and vibrational states of H atoms in bulk Pd metal and nanocrystalline Pd metal.[22] The activated H species on metals or metal particles have been studied by INS to elucidate the dynamics of the H species and the catalysis involved.[21,23–26] INS was utilized to discriminate the vibrational modes of H species on different adsorption sites of the Pt particles immobilized on a carbon support, which was correlated with the specific electrocatalytic activity.[26] Recently, the active H species on a 5 wt% Pt/C catalyst were detected by INS.[27] Evidence of the H spillover from Pt to unsaturated reactive sites in the carbon was also provided. In the case of a Au/CeO_2, the heterolytic bond cleavage of H_2 has been reported by the combination of INS and FT-IR.[28] In a recent study, Pt–H species with *n*-fold coordination were detected on a Pt/Al_2O_3 catalyst by INS.[29] These recent results have demonstrated that the INS technique is effective to detect active H species on supported metal catalysts. However, the individual assignment of each H species on catalysts is still a challenge in the field of catalytic science.

In this study, we tackled this challenging issue, specifically, individual identification of each H species on a Pt/Al_2O_3 catalyst in the ethylene hydrogenation reaction using *in situ* INS. We successfully identified several H species on the Pt particles and H species that migrated from the Pt particles to the Al_2O_3 support by the combination of *in situ* INS and density functional theory (DFT) calculations for the first time. In addition, we demonstrated that the Pt–H at atop sites, the Pt–H–Pt at bridged perimeter and terrace sites, and Pt_3–H at threefold sites were active intermediates in C_2H_4 hydrogenation by the *in situ* INS and FT-IR.

Experimental

Preparation of 5 wt% Pt/Al_2O_3 catalysts

An aqueous nitric acid solution containing *cis*-[$Pt(NH_3)_2(NO_2)_2$], in which the content of Pt was 4.64 wt%, was purchased from Furuya Metal Corporation Ltd. γ-Al_2O_3 (JRC-ALO-7) of 180 m^2 g^{-1} was provided by the Catalysis Society of Japan. A Pt/Al_2O_3 catalyst was prepared by an impregnation method. The loading amount of Pt was 5.0 wt% as a metal basis. γ-Al_2O_3 (10 g) was added to an aqueous solution (100 mL) containing *cis*-[$Pt(NH_3)_2(NO_2)_2$] solution (11.3 g), followed by solvent evaporation at 80 °C. The resulting powder was calcined in air at 673 K for 5 h. Thus-obtained catalyst was reduced under a H_2 gas flow (5% H_2/N_2, 50 mL min^{-1}) at 623 K for 2 h.

Structural characterization

Crystal structure of the Pt/Al_2O_3 was analysed by a Ultima IV X-ray diffractometer (Rigaku, Japan). The local structure of the Pt/Al_2O_3 was investigated by X-ray absorption fine structure (XAFS). XAFS measurements were performed at the BL01B1 beamline of SPring-8 facility of the Japan Synchrotron Radiation Research Institute. A Si(111) double-crystal monochromator was used to obtain the incident X-ray beam. Pt L_3-edge XAFS spectra of Pt foil and the Pt/Al_2O_3 were recorded in transmission mode using ionization chambers at room temperature in air and He, respectively. Energy was calibrated using Pt foil. Before the XAFS measurement of the Pt/Al_2O_3, it was heated at 673 K under 5% H_2/He (flow rate: 100 mL min^{-1}) conditions for 1 h. XAFS spectra were analyzed using a xTunes software.[30] After normalization, k^3-weighted χ spectra in the k range of 3.0–16.0 $Å^{-1}$ were Fourier-transformed into r space to obtain FT-EXAFS spectra. The curve fitting analysis was conducted in the range of 1.9–2.9 Å using a FEFF8 program.[31]

Catalytic reactions

Ethylene hydrogenation reaction was carried out using a fixed-bed flow reactor at 303 K. In this experiment, the total flow rate of gas was fixed to 100 mL min^{-1}. Before the activity test, the Pt/Al_2O_3 catalyst (10.3 mg) was reduced by 5% H_2/He at 473 K for 60 min, and then the reaction gas mixture of H_2(5%)/C_2H_4(5%)/He was introduced into the reactor. At 60 min after the start of the reaction, H_2 gas was removed from the reaction gas [*i.e.*, C_2H_4(5%)/He] and then introduced again after 120 min. The conversion of ethylene was calculated from the following equation:

$$\text{Conversion of ethylene} = (X_{in} - X_{out})/X_{in} \quad (1)$$

where X_{in} and X_{out} are the concentrations of ethylene gas in the inlet and outlet gases, respectively.

FT-IR measurements

In situ diffuse reflectance infrared Fourier-transform (DRIFT) spectra were obtained using an ISDR-600 FT-IR spectrometer (JASCO, Japan) equipped with a mercury–cadmium–tellurium (MCT) at a resolution of 4 cm^{-1} with 64 co-added scans. Diffuse reflectance cell was filled with the sample power and sealed with a KBr window from the top. In this experiment,

the total flow rate of the reaction gas was fixed to 50 mL min^{-1}. The Pt/Al_2O_3 sample was pretreated in a flow of 5% H_2/He for 30 min at 473 K and then cooled to room temperature under a He atmosphere. After measurement of the background spectrum at 303 K under a He atmosphere, the DRIFT spectra were obtained under the gas flow conditions of H_2(5%)/He, H_2(5%)/C_2H_4(5%)/He, and C_2H_4(5%)/He.

Inelastic neutron scattering measurements

The inelastic neutron scattering measurements were carried out with the 4SEASONS time-of-flight spectrometer, SIKI, at the MLF, J-PARC, Japan.[32] The samples were loaded into thin double-walled cells whose shape was a traditional hollow cylindrical design, but had gas inlet and outlet cocks added to the top and bottom of the cell. The internal space of the inner cylinder had a hole to contain the same atmosphere of the cryostat exchange gas, to reduce the background contribution as much as possible.

The reduced catalyst was tableted, pulverized to a 50–100 mesh and set in the measurement cell. Before the INS experiments, the sample cells were connected to a pretreatment/reaction system, and were vacuumed and heated (up to 473 K); then, gas (5% H_2/He) was flowed to remove a surface oxide layer on the Pt metal nanoparticles at a sample preparation room on the offsite of the neutron beamline. After cooling the samples to 300 K, the reaction gas (5% H_2/He, 5% C_2H_4/He, (5% H_2 + 5% C_2H_4)/He) or He gas (flow rate: 50 ml min^{-1}) was introduced into the cell. After reacting for 1 h, the gas cocks were closed and then the cell was attached to the sample stick of the cryostat for the neutron spectrometer.

The spectrometer has multiple incident energy (E_i) capability.[33] The Fermi chopper frequency was 300 Hz and setting E_i was 150 meV. Typical energy resolutions were about ΔE = ~1 meV at $\hbar\omega$ of 50–60 meV and ~4 meV at 80–100 meV, respectively. Data collection was performed at 123 K, facilitated by the 4SEASONS cryostat and counted for 6–12 h. Data reduction and analysis were carried out using the software package Utsusemi.[34] The INS spectra were obtained with integrated $\boldsymbol{Q}$ in the range of $2 \leq |\boldsymbol{Q}| \leq 10$ $Å^{-1}$. Throughout this paper, the error bar in the spectra represents the standard deviation.

DFT calculations

DFT calculations were performed to identify the active hydrogen species and to assign the INS spectra. We employed a periodic slab model of the γ-alumina (110) surface with loading of a Pt rod. The supercell contains an $(Al_2O_3)_{16}$ unit as proposed by Pinto *et al.*[35] with six-layer thickness. A two-layer rod-like Pt(111) structure is put on the alumina surface: the bottom layer involves a hexagonal Pt_8 unit and a Pt_6 unit constructs the top layer. The model contains $Pt_{14}(Al_2O_3)_{16}$ in each supercell. We inserted a vacuum space of 20 Å above the surface and optimized all of the cell parameters and the position of ions. Spin-polarized DFT calculations were performed with the PW91 function[36] implemented with the projector augmented wavefunction (PAW) method for representing the core electrons.[37,38] We used a 2 × 2 × 1 Γ-centred *k*-point mesh. The plane-wave cut-off was set to 600 eV, which is the optimal value to satisfy the energy convergence. On the optimized Pt/Al_2O_3 structure, hydrogen atoms were adsorbed. We fixed the ionic position of the bottom two layers during the calculations of hydrogen adsorption and vibrations. The DFT calculations were performed using the VASP package.[39,40] The spectrum simulation was performed using the oClimax program.[41] The atomic charges on H atoms were evaluated according to Bader partitioning.[42]

Results

Hydrogenation of ethylene on Pt/Al_2O_3

XRD patterns of the prepared 5 wt% Pt/Al_2O_3 sample and the bare Al_2O_3 sample revealed that Pt metal species was highly dispersed on the Al_2O_3 support because of no diffraction peaks assigned to Pt species (Fig. S1†). Pt L_3-edge XANES spectrum of the Pt/Al_2O_3 (Fig. S2a†) revealed that the metallic Pt species was formed on Al_2O_3 after H_2 treatment because the absorption peak (electron transition from Pt 2p to Pt 5d) intensity of Pt/Al_2O_3 at 11 567.5 eV was similar to that of Pt foil. The particle size of the supported Pt was estimated to be 1–2 nm from the CN (5.7 ± 0.3) of Pt–Pt, which was obtained by the curve fitting analysis of FT-EXAFS spectrum of the Pt/Al_2O_3 (Fig. S2b, Table S1†). This value was in good accordance with the Pt particle size (1.8 nm) of the Pt/Al_2O_3 determined by the CO pulse method using BELCAT-B (MicrotracBEL Corp., Japan).

The ethylene hydrogenation reaction was carried out over a 5 wt% Pt/Al_2O_3 catalyst at 303 K. Fig. 1 shows the time course of the conversion of ethylene with H_2 [(a) 0–60 min, (c) 120–150 min] and without it [(b) 60–120 min] over the Pt/

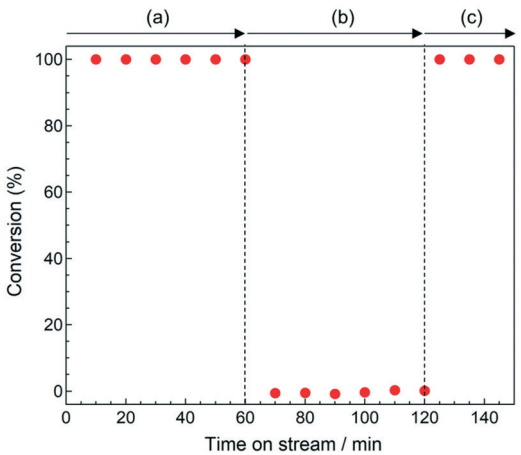

Fig. 1 Catalytic hydrogenation of ethylene using the 5 wt% Pt/Al_2O_3 catalyst at 303 K (a) under H_2(5%)/C_2H_4(5%)/He, (b) under C_2H_4(5%)/He, and (c) under H_2(5%)/C_2H_4(5%)/He.

Al_2O_3 catalyst. Ethylene conversion of >99% was achieved in the presence of H_2 and ethane was formed (Fig. 1a and c). On the other hand, the ethylene conversion was suppressed in the absence of H_2 (Fig. 1b). In the presence of H_2, the H species, which is generated by the activation of H_2 on the Pt particles, reacted with ethylene to form ethane at 303 K. However, dehydrogenation reaction did not proceed at 303 K because the free energy change of the ethylene dehydrogenation is large (141 kJ mol^{-1}).[43]

Fig. 2 shows the *in situ* DRIFT spectra of the Pt/Al_2O_3 sample under several gas conditions. The addition of H_2 increased the intensity of the bands at 2041 and 2112 cm^{-1} (Fig. 2a), which are assigned to on-top hydride and atop H species on the Pt surface, respectively, based on the previous reports.[29,44–46] We could not detect the *n*-fold H species because of the selection rule of IR spectroscopy.[29] The bands in the regions of 1600–1750 and 3100–3700 cm^{-1}, which are attributed to Al–OH species, appeared upon the introduction of H_2. This phenomenon is explained by the H spillover from the Pt surface to the Al_2O_3 surface.[45] In the presence of C_2H_4 without H_2, π-CH_2=CH_2 (1200 and 1490 cm^{-1}) and ethylidyne (1339 and 2883 cm^{-1}) on the Pt surface were detected (Fig. 2b) along with the absorption bands of gaseous C_2H_4 at 1444, 1889, 2989, 3086 and 3131 cm^{-1}.[47–49] In addition, the formation of Al–OH species was also observed in the absence of H_2 gas. Since the reactivity of π-CH_2=CH_2 is higher than that of ethylidyne in the C_2H_4 hydrogenation reaction,[50] the Al–OH species would be formed by the migration of H species, which were generated in the ethylidyne formation process on the Pt surface as shown in reaction (2).

$$Pt + CH_2{=}CH_2 \rightarrow CH_3C{-}Pt\ (\text{ethylidyne}) + H_{ads} \qquad (2)$$

The H species on the Pt surface were not detected in the region of 2000–2150 cm^{-1} under the C_2H_4 atmosphere without H_2 (Fig. 2b) because reaction (2) is suppressed by the saturation of ethylidyne species on the proper Pt sites.[51] In the presence of both C_2H_4 and H_2 (Fig. 2c), gaseous product C_2H_6 was detected at 1400–1550, 2775 and 2840–3100 cm^{-1} overlapping with the small amount of unreacted C_2H_4.[47,52] The signal intensities of hydride (2046 cm^{-1}), H species (2118 cm^{-1}) and π-CH_2=CH_2 (1200 and 1490 cm^{-1}) on the Pt surface in Fig. 2c were weakened compared to those in Fig. 2a and b because these species were consumed in the C_2H_4 hydrogenation reaction, which is in good accordance with previous works.[29,44,48]

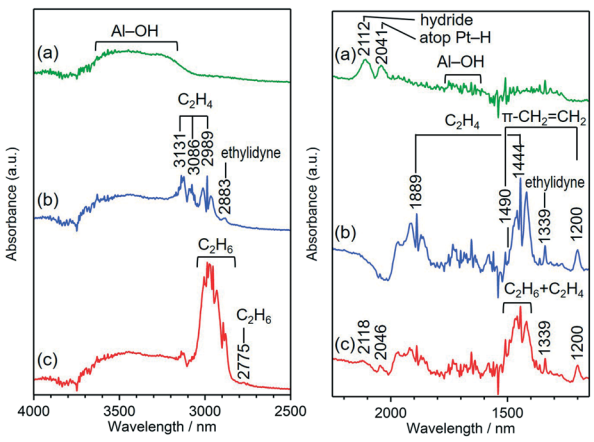

Fig. 2 *In situ* DRIFT spectra of the 5 wt% Pt/Al_2O_3 sample (a) under H_2(5%)/He, (b) under C_2H_4(5%)/He, (c) under H_2(5%)/C_2H_4(5%)/He. The background was obtained using Pt/Al_2O_3 under He at 303 K after the H_2 pretreatment.

Observation of adsorbed hydrogen species on Pt/Al_2O_3 by INS

Identification of the H species that are silent for FT-IR and investigation of their reactivity are crucial to understand the ethylene hydrogenation catalysis.[29] To achieve this goal, INS measurements were performed at the BL01 beamline "4SEASONS" of J-PARC. To determine the motions and positions of atoms, INS is the unique technique, in particular for light atoms, *e.g.* H, Li, and so on. Fig. 3A shows the typical powder averaged color contour map of INS intensity of the 5 wt% Pt/Al_2O_3 sample treated with H_2, as functions of momentum transfer vector $\boldsymbol{Q}$ (space correlation information) and energy transfer $\hbar\omega$ (time correlation information) measured at 123 K with E_i = 150 meV. In powder sample, only the information of radial direction (momentum transfer vector $\boldsymbol{Q}$) is available and crystal orientations are sacrificed by the integration of powder averaged. Due to the nature of

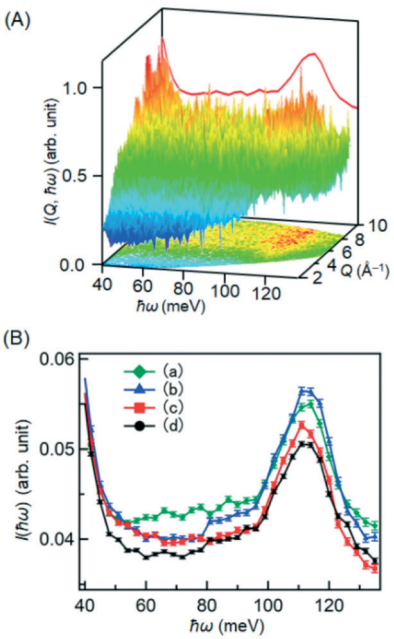

Fig. 3 (A) Powder averaged INS intensity contour map and INS spectrum of 5 wt% Pt/Al_2O_3 with 5% H_2 (He balance) measured at T = 123 K with E_i = 150 meV. (B) *In situ* INS spectra of (a) 5 wt% Pt/Al_2O_3 with 5% H_2 (He balance), (b) 5 wt% Pt/Al_2O_3 with 5% C_2H_4 (He balance), (c) 5 wt% Pt/Al_2O_3 with 5% C_2H_4 and 5% H_2 (He balance), and (d) 5 wt% Pt/Al_2O_3 with He.

incoherent scattering of hydrogen, INS spectrum can be integrated over the $\boldsymbol{Q}$ range further, in this case 2–10 $Å^{-1}$ (red spectrum in Fig. 3A), to obtain the better statistics of the INS intensities.

Fig. 3B shows the INS spectra of Pt/Al_2O_3 measured at several conditions. In the spectrum for the Pt/Al_2O_3 sample without H_2 (Fig. 3Bd), a peak was observed in the range of 100–120 meV, which is attributed to surface OH groups on the support (discussed later). The intensity increased in the wide range of 50–120 meV due to the presence of H_2, as shown in Fig. 3Ba. These signals were not detected for the bare Al_2O_3 support treated with H_2 (Fig. S3†). Therefore, the signals in 50–120 meV would be assigned to the hydrogen species produced by the Pt metal catalyst and adsorbed on the Pt surface, the Al_2O_3 support, and the interface between them. These signals in the region of 50–120 meV were reduced by the addition of C_2H_4 (Fig. 3Bc). This drastic change is due to the reaction of C_2H_4 with the H species on the Pt, the Al_2O_3 surfaces, and/or the interface between them. The signal intensities were also increased in the C_2H_4 atmosphere without H_2, as shown in Fig. 3Bb, indicating that the H species are formed on the Pt/Al_2O_3 sample according to reaction (2). The signal intensities of H species at 80–120 meV were as high as those for the Pt/Al_2O_3 sample in the H_2 atmosphere, whereas the intensities at 60–80 meV were similar to those obtained after the reaction of $C_2H_4 + H_2$ in Fig. 3Bc.

DFT calculation of activated H species on Pt/Al_2O_3 and simulation of INS spectrum

DFT calculations were employed to determine feasible adsorption structures of single H atom on the Pt/Al_2O_3 catalyst using the supercell of $Pt_{14}(Al_2O_3)_{16}$ as a model of the Pt/Al_2O_3 surface structure. We performed the geometry optimization using probable initial structures that involves atop and bridge sites on Al_2O_3, atop, bridge, and threefold sites on Pt, and Pt/Al_2O_3 perimeter sites. The representative adsorption structures obtained by geometry optimization are shown in Fig. 4a and Table S2,† and categorized as follows. Five binding structures were found on the Al_2O_3 surface: AlO–H (1–3) and bridged Al–H–Al (4,5), whereas three structures were observed on the Pt_{14} moiety: bridged Pt–H–Pt at the terrace (6), edge (7) and perimeter (8) sites. We also found threefold Pt_3–H structures at the face-centered cubic (fcc)-like hollow site Pt_3–H_{fcc} (9), where a Pt atom exists directly below the site, and the hexagonal close-packed (hcp)-like hollow site Pt_3–H_{hcp} (10) without a Pt atom below the site. The H atoms of AlO–H (1–3) and Al–H–Al (4,5) were assigned to proton and hydride, respectively (Table S3†). Atomic (neutral) hydrogen was found on Pt–H–Pt (6,7), Pt_3–H_{fcc} (9) and Pt_3–H_{hcp} (10), whereas the perimeter Pt–H–Pt (8) involved a slightly negative charge, indicating a hydride-like character (Table S3†). The binding structures similar to terrace Pt–H–Pt (6), edge Pt–H–Pt (7) and threefold Pt_3–H_{fcc}

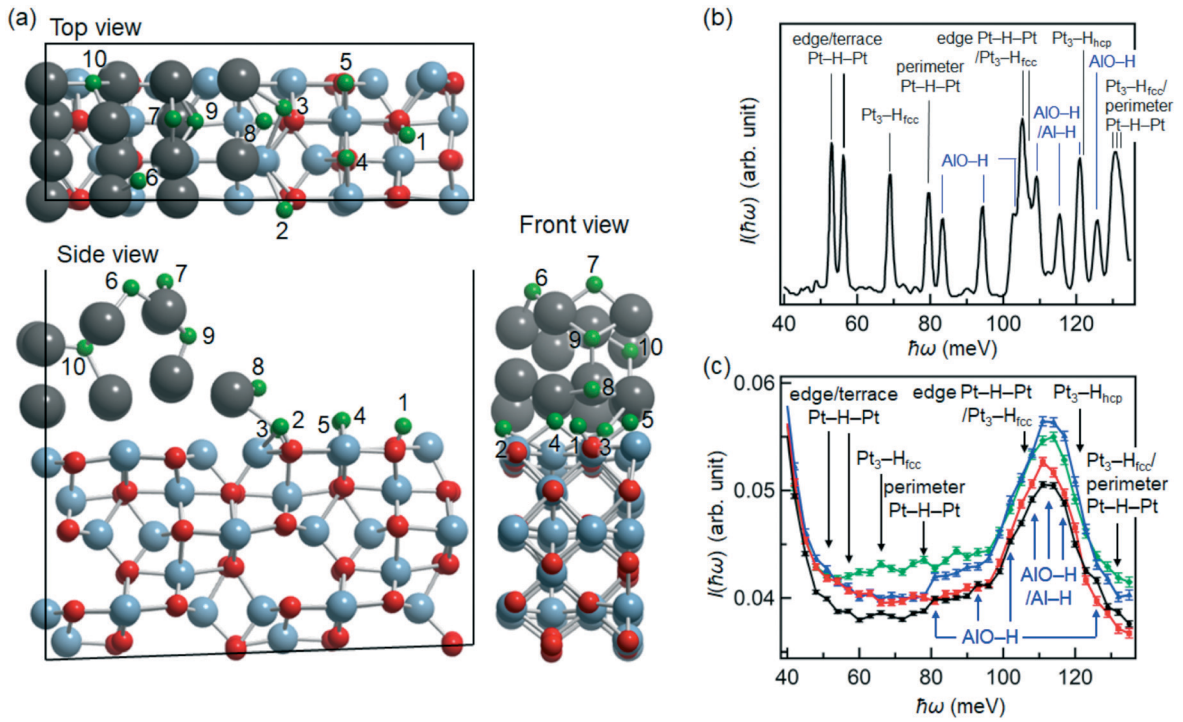

Fig. 4 (a) Optimized structure of ten H atoms on the supercell of $Pt_{14}(Al_2O_3)_{16}$ (H: green, Pt: grey, Al: light blue, O: red). The adsorption sites of H atoms are shown as follows: (1) AlO–H, (2) AlO–H, (3) AlO–H, (4) bridge Al–H–Al, (5) bridge Al–H–Al, (6) terrace Pt–H–Pt, (7) edge Pt–H–Pt, (8) perimeter Pt–H–Pt, (9) threefold Pt_3–H_{fcc} and (10) threefold Pt_3–H_{hcp}. (b) Simulated INS spectrum of ten H atoms on the supercell of $Pt_{14}(Al_2O_3)_{16}$. (c) Assignment of the experimental INS spectra.

(9) have been previously reported on a Pt_{127}/(100)MgO model structure.[53] After the geometry optimization, however, the initial structure of atop Pt–H transferred to a more stable bridged structure. This is because the Pt surface structures and coverage of adsorbed H strongly affect the H adsorption energy at each site.[53–56]

The vibrational frequencies of the H-adsorbed Pt/Al_2O_3 were calculated using the structure in Fig. 4a. We assumed high coverage of H species on the catalyst and therefore considered ten H atoms of representative adsorption structures. The structure of $(H)_{10}Pt_{14}(Al_2O_3)_{16}$ was optimized again. Table S4† summarizes the calculated frequency and assignments of vibrational modes. The AlO–H stretching frequencies were at 300–450 meV. The frequencies of the Pt–H and Al–H stretching modes at bridge sites were calculated to be in the range of 160–180 meV whereas those of the AlO–H bending modes, Al–H bending modes coupled with AlO–H bending and Pt–H stretching modes at threefold sites were in the range of 100–150 meV. The coupled vibrations of Pt–H stretching modes between threefold and bridge (edge, terrace, perimeter) sites also appeared in this energy region. At 50–100 meV, the bending modes of AlO–H and Pt–H were obtained. The vibrations of the Al_2O_3 framework were calculated at lower than 100 meV. The simulated INS spectrum (at 0 K) using the DFT results is shown in Fig. 4b: the peak intensities are

$$I(\hbar\omega) = \int \mathrm{d}Q \frac{\hbar^2 Q^2}{6M\omega} \exp\left(-\langle u^2\rangle Q^2\right) G(\omega) \left[\left\{\exp\left(\frac{\hbar\omega}{kT}\right) - 1\right\}^{-1} + 1\right] \quad (3)$$

where M is the mass of scattering atoms, ω is the vibrational frequency, $\langle u^2\rangle$ is the atomic mean-square displacement, and T is the temperature.[41] The factor $G(\omega)$ is the density of vibrational state that depends on the number of adsorbed species in the model. Since we considered one model structure only, the peak intensities are just guide. We found that only vibrational modes involving H atoms exhibited high intensity. Because the intensity of the INS spectrum is in inverse proportion to the mass of scattering atoms, the vibrations of the Al_2O_3 framework exhibited only a relatively low intensity. On the basis of these model calculations, we assigned the INS spectrum as shown in Fig. 4c. Major reasons for the discrepancies between Fig. 4b and c are the limited number of adsorbed structures considered in our model and lack of information on the populations of individual binding modes.

Carosso *et al.* reported that the H species on a Pt/Al_2O_3 sample in the presence of H_2 were detected at 58.2, 66.3, 73.1, 83.0 and 92.9 meV in the INS spectrum.[29] We presented their results in the region of 40–100 meV. They expected that these signals are assigned to *n*-fold (bridged, hollow and fourfold coordinated) Pt–H species. In the present study, we demonstrated that the H species are not only the Pt–H species [edge, terrace, perimeter Pt–H–Pt (6–8), Pt_3–H_{fcc} (9), Pt_3–H_{hcp} (10)], but also AlO–H (1–3) and Al–H–Al (4,5) species, as shown in Fig. 4c. In addition, we successfully identified that the signals appearing at 100–130 meV are mainly assigned to AlO–H (1–3) and Al–H–Al (4,5) species, although these signals were not mentioned in the previous study.[5]

Discussion

Activated surface species of H_2 and C_2H_4 on Pt/Al_2O_3 catalyst

We summarized the activated H species on Pt/Al_2O_3 obtained by INS and FT-IR spectroscopies in Scheme 1a. We demonstrated the formation of surface H species [edge and terrace Pt–H–Pt (6,7), Pt_3–H_{fcc} (9), and Pt_3–H_{hcp} (10)], which has been predicted by DFT calculations using model Pt structures,[53–57] on the Pt/Al_2O_3 surface in the presence of H_2 by the INS and DFT (Fig. 3B and 4c) in this study. In addition, the perimeter Pt–H–Pt (8) at the interface between Pt particles and Al_2O_3 support was also detected in H_2 conditions.

We found some AlO–H (1–3) and Al–H–Al (4,5) species on the Pt/Al_2O_3 sample even in the He condition, in contrast to the bare Al_2O_3 in the presence of H_2, as shown in Fig. S3.† The introduction of H_2 during the pretreatment should generate the additional AlO–H (1–3) and Al–H–Al (4,5) species (Fig. 3Ba). It is reported that H species travel a short distance from the Pt surface to the Al_2O_3 surface.[5] This H spillover from Pt particles gives the AlO–H (1–3) and Al–H–Al (4,5) species (Scheme 1a), which is consistent with the fact that the AlO–H (1–3) and Al–H–Al (4,5) species were not detected on the bare Al_2O_3 support, even in the presence of H_2 (Fig. S3†).

The C_2H_4 provided not only adsorbed π-CH_2═CH_2 and ethylidyne, but also AlO–H and Al–H–Al species on the Pt/Al_2O_3 catalyst, which is evidenced by the FT-IR and INS studies as shown in Scheme S1.† In addition, the edge and/or terrace Pt–H–Pt (6 and/or 7) species appearing at 50–55 meV in Fig. 3Bb were detected despite the absence of H_2. Tan

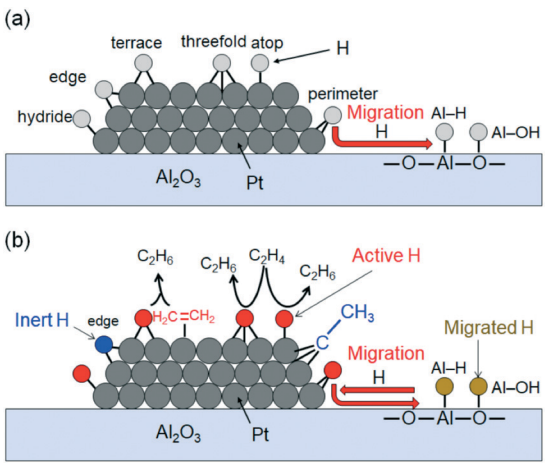

Scheme 1 (a) Activated H species on Pt/Al_2O_3 in the presence of H_2. (b) Reaction mechanism of active H species on Pt/Al_2O_3 in C_2H_4 hydrogenation.

et al. reported that the H adsorption on a bridged terrace site is unstable and requires high H_2 coverage on the Pt surface.[54] On the other hand, the edge site is strongest adsorption site in the ridged Pt surface.[55] Furthermore, the H adsorption on the edge site is favourable in the model of H-covered Pt_{127}/(100)MgO.[53] Therefore, the Pt–H species formed at 50–55 meV is edge Pt–H (Scheme S1†). This means that the H species generated through the formation of ethylidyne are stored on both the Pt and Al_2O_3 surfaces.

Active H species on Pt/Al_2O_3 for C_2H_4 hydrogenation reaction

The perimeter Pt–H–Pt (8), Pt_3–H_{fcc} (9), and hydride and atop Pt–H species appearing in the presence of H_2 were drastically reduced by the addition of C_2H_4 with the decrease in the peak intensities of π-CH_2═CH_2 (1200 and 1490 cm^{-1}), which is the active species in the C_2H_4 hydrogenation reaction.[50] These results indicate that the perimeter Pt–H–Pt (8), Pt_3–H_{fcc} (9), and hydride and atop Pt–H species can react with π-CH_2═CH_2 [Langmuir–Hinshelwood (L–H) reaction mechanism] and gaseous C_2H_4 [Eley–Rideal (E–R) reaction mechanism][58] to form C_2H_6 (Scheme 1b). In addition, the signal intensity at 55–60 meV also decreased upon the introduction of C_2H_4 (Fig. 3Ba and c). This signal is attributed to terrace Pt–H–Pt (6), which is unstable on the Pt surface.[54,56] Thus, the terrace Pt–H–Pt (6) is also an active species in the C_2H_4 hydrogenation reaction (Scheme 1b). On the other hand, the edge Pt–H–Pt (7) was still observed after the C_2H_4 hydrogenation reaction (Fig. 3Bc). The edge Pt–H–Pt (7) is the most stable species on the ridge Pt surface.[55] The strong interaction between H and Pt on the edge site inhibits the reaction of edge Pt–H–Pt (7) with C_2H_4.

The additionally formed AlO–H (1–3) and Al–H–Al (4,5) in the presence of H_2 or C_2H_4 were not observed after the reaction of C_2H_4 and H_2, although these AlO–H (1–3) and Al–H–Al (4,5) could not react with C_2H_4 directly (Fig. 3B). Thus, the H species on Al_2O_3, provided by H_2 and/or C_2H_4, can re-migrate to the Pt particle to react with C_2H_4 under the reaction conditions (Scheme 1b), whereas the H species strongly adsorbed on Al_2O_3, which remained even in the He condition (Fig. S3†), cannot re-migrate. It was reported that the metal–organic frameworks[59] and carbons[60] acted as a hydrogen storage material *via* the H spillover from supported Pt and Pd particles, as revealed by H_2 adsorption/desorption experiments. In addition, H species were provided from metal to carbon materials through Al_2O_3 in the case of Pd/Al_2O_3-decorated graphene sheet.[61] The present study provides evidence that the Al_2O_3 support itself also acts like a hydrogen store and the formed AlO–H (1–3) and Al–H–Al (4,5) can be used as H sources in the C_2H_4 hydrogenation reaction.

Conclusions

In summary, we demonstrated that the H species such as bridged Pt–H–Pt (edge, terrace, perimeter), three-fold Pt_3–H, AlO–H, and bridged Al–H–Al species on Pt/Al_2O_3 catalyst were identified by the combination of INS spectroscopy and DFT calculations for the first time. The reactivity of the H species was successfully observed by *in situ* INS and FT-IR. The atop and hydride Pt–H, terrace and perimeter Pt–H–Pt (6,8), Pt_3–H_{fcc} (9) and Pt_3–H_{hcp} (10) were active intermediates in C_2H_4 hydrogenation to produce C_2H_6 *via* L–H and/or E–R reaction mechanisms whereas the edge Pt–H–Pt (7) was inert species in the C_2H_4 hydrogenation. In addition, we obtained the direct evidence that the Al_2O_3 support itself acted as a hydrogen storage material and the formed AlO–H (1–3) and Al–H–Al (4,5) species can be used as H sources in the C_2H_4 hydrogenation reaction. This hydrogen storage property should also contribute to the catalytic activity. The results obtained in this study provide the significant insights for the elucidation of reaction mechanism of the catalytic hydrogenation reactions.

Conflicts of interest

There are no conflicts to declare.

Acknowledgements

This work was supported by the Elements Strategy Initiative for Catalysts and Batteries (ESICB) of MEXT, grant number JPMXP0112101003. The INS experiments were performed with the approval of Japan Proton Accelerator Research Complex (J-PARC) (Proposal No. 2019A0091, 2017E0003, 2017B0229, 2015E0004 and 2013B0093). XAFS experiments were conducted at SPring-8 with the approval of the Japan Synchrotron Radiation Research Institute (JASRI) (Proposal numbers: 2018A1497 and 2018B1352). The computations were performed at the Research Center for Computational Science, Okazaki, Japan.

Notes and references

1 F. Zaera, *Phys. Chem. Chem. Phys.*, 2013, **15**, 11988–12003.
2 D. Wang and D. Astruc, *Chem. Rev.*, 2015, **115**, 6621–6686.
3 J. A. Delgado, O. Benkirane, C. Claver, D. Curulla-Ferré and C. Go-dard, *Dalton Trans.*, 2017, **46**, 12381–12403.
4 F. Meemken and A. Baiker, *Chem. Rev.*, 2017, **117**, 11522–11569.
5 F. Zaera, *ACS Catal.*, 2017, **7**, 4947–4967.
6 R. Ye, A. V. Zhukhovitskiy, C. V. Deraedt, F. D. Toste and G. A. Somorjai, *Acc. Chem. Res.*, 2017, **50**, 1894–1901.
7 L. Zhang, M. Zhou, A. Wang and T. Zhang, *Chem. Rev.*, 2020, **120**, 683–733.
8 P. Kluson, *Appl. Catal., A*, 1995, **128**, 12–31.
9 J. Harris and S. Andersson, *Phys. Rev. Lett.*, 1985, **55**, 1583–1586.
10 G. D. Frey, V. Lavallo, B. Donnadieu, W. W. Schoeller and G. Ber-trand, *Science*, 2007, **316**, 439–441.
11 S. Klacar and H. Grönbeck, *Catal. Sci. Technol.*, 2013, **3**, 183–190.
12 E. D. German, H. Abir and M. Sheintuch, *J. Phys. Chem. C*, 2013, **117**, 7475–7486.

13 F. Ahmed, M. K. Alam, A. Suzuki, M. Koyama, H. Tsuboi, N. Hatakeyama, A. Endou, H. Takaba, C. A. Del Carpio, M. Kubo and A. Miyamoto, *J. Phys. Chem. C*, 2009, **113**, 15676–15683.
14 R. Prins, *Chem. Rev.*, 2012, **112**, 2714–2738.
15 W. Karim, C. Spreafico, A. Kleibert, J. Gobrecht, J. VandeVondele, Y. Ekinci and J. A. van Bokhoven, *Nature*, 2017, **541**, 68.
16 T. Mitsudome, Y. Mikami, M. Matoba, T. Mizugaki, K. Jitsukawa and K. Kaneda, *Angew. Chem., Int. Ed.*, 2012, **51**, 136–139.
17 Y. Cao, Z. Sui, Y. Zhu, X. Zhou and D. Chen, *ACS Catal.*, 2017, **7**, 7835–7846.
18 P. G. Savva and C. N. Costa, *Catal. Rev.: Sci. Eng.*, 2011, **53**, 91–151.
19 V. F. Sears, *Neutron News*, 1992, **3**, 26–37.
20 A. Pawlukojć, I. Natkaniec, E. Grech, J. Baran, Z. Malarski and L. Sobczyk, *Spectrochim. Acta, Part A*, 1998, **54**, 439–448.
21 P. W. Albers, G. Prescher, K. Seibold and S. F. Parker, *Chem. Eng. Technol.*, 1999, **22**, 135–137.
22 M. Kofu, N. Hashimoto, H. Akiba, H. Kobayashi, H. Kitagawa, K. Iida, M. Nakamura and O. Yamamura, *Phys. Rev. B*, 2017, **96**, 054304.
23 P. W. Albers, E. Auer, K. Ruth and S. F. Parker, *J. Catal.*, 2000, **196**, 174–179.
24 P. W. Albers, M. Poniatowski, S. F. Parker and D. K. Ross, *J. Phys.: Condens. Matter*, 2000, **12**, 4451–4463.
25 P. W. Albers, J. Pietsch, J. Krauter and S. F. Parker, *Phys. Chem. Chem. Phys.*, 2003, **5**, 1941–1949.
26 P. W. Albers, M. Lopez, G. Sextl, G. Jeske and S. Parker, *J. Catal.*, 2004, **223**, 44–53.
27 M. Carosso, A. Lazzarini, A. Piovano, R. Pellegrini, S. Morandi, M. Manzoli, J. G. Vitillo, M. Jimenez Ruiz, C. Lamberti and E. Grop-po, *Faraday Discuss.*, 2018, **208**, 227–242.
28 R. Juárez, S. F. Parker, P. Concepción, A. Corma and H. García, *Chem. Sci.*, 2010, **1**, 731–738.
29 M. Carosso, E. Vottero, A. Lazzarini, S. Morandi, M. Manzoli, K. A. Lomachenko, M. J. Ruiz, R. Pellegrini, C. Lamberti, A. Pio-vano and E. Groppo, *ACS Catal.*, 2019, **9**, 7124–7136.
30 H. Asakura, S. Yamazoe, T. Misumi, A. Fujita, T. Tsukuda and T. Tanaka, *Radiat. Phys. Chem.*, 2020, **175**, 108270.
31 A. L. Ankudinov, B. Ravel, J. J. Rehr and S. D. Conradson, *Phys. Rev. B: Condens. Matter Mater. Phys.*, 1998, **58**, 7565.
32 R. Kajimoto, M. Nakamura, Y. Inamura, F. Mizuno, K. Nakajima, S. O. Kawamura, T. Yokoo, T. Nakatani, R. Maruyama, K. Soyama, K. Shibata, K. Suzuya, S. Sato, K. Aizawa, M. Arai, S. Wakimoto, M. Ishikado, S. Shamoto, M. Fujita, H. Hiraka, K. Ohoyama, K. Yamada and C. H. Lee, *J. Phys. Soc. Jpn.*, 2011, **80**, SB025.
33 M. Nakamura, R. Kajimoto, Y. Inamura, F. Mizuno, M. Fujita, T. Yokoo and M. Arai, *J. Phys. Soc. Jpn.*, 2009, **78**, 093002.
34 Y. Inamura, T. Nakatani, J. Suzuki and T. Otomo, *J. Phys. Soc. Jpn.*, 2013, **82**, SA031.
35 H. P. Pinto, R. M. Nieminen and S. D. Elliott, *Phys. Rev. B: Condens. Matter Mater. Phys.*, 2004, **70**, 125402.
36 J. P. Perdew, J. A. Chevary, S. H. Vosko, K. A. Jackson, M. R. Pederson, D. J. Singh and C. Fiolhais, *Phys. Rev. B: Condens. Matter Mater. Phys.*, 1992, **46**, 6671–6687.
37 P. E. Blöchl, *Phys. Rev. B: Condens. Matter Mater. Phys.*, 1994, **50**, 17953–17979.
38 G. Kresse and D. Joubert, *Phys. Rev. B: Condens. Matter Mater. Phys.*, 1999, **59**, 1758–1775.
39 G. Kresse and J. Furthmüller, *Phys. Rev. B: Condens. Matter Mater. Phys.*, 1996, **54**, 11169–11186.
40 G. Kresse and J. Furthmüller, *Comput. Mater. Sci.*, 1996, **6**, 15–50.
41 K. Ramić, C. Wendorff, Y. Cheng, A. I. Kolesnikov, D. L. Aber-nathy, L. Daemen, G. Arbanas, L. Leal, Y. Danon and L. Liu, *Ann. Nucl. Energy*, 2018, **120**, 778–787.
42 G. Henkelman, A. Arnaldsson and H. Jónsson, *Comput. Mater. Sci.*, 2006, **36**, 354–360.
43 F. Cataldo, *J. Photochem. Photobiol., A*, 1996, **99**, 75–81.
44 Y. Soma, *J. Catal.*, 1979, **59**, 239–247.
45 M. Haneda, T. Watanabe and M. Ozawa, *J. Jpn. Pet. Inst.*, 2012, **55**, 191–196.
46 Y. Dong, G. Hu, X. Hu, G. Xie, J. Lu and M. Luo, *J. Phys. Chem. C*, 2013, **117**, 12537–12543.
47 G. B. Lebron and T. L. Tan, *Int. J. Spectrosc.*, 2012, **2012**, 474639.
48 M. K. Ko and H. Frei, *J. Phys. Chem. B*, 2004, **108**, 1805–1808.
49 W. Wasylenko and H. Frei, *J. Phys. Chem. B*, 2005, **109**, 16873–16878.
50 T. Miura, H. Kobayashi and K. Domen, *J. Phys. Chem. B*, 2000, **104**, 6809–6814.
51 J. Kubota, S. Ichihara, J. N. Kondo, K. Domen and C. Hirose, *Langmuir*, 1996, **12**, 1926–1927.
52 FT-IR data of ethane, NIST Chemistry WebBook, Standard Reference Database 69.
53 S. M. Kozlov, H. A. Aleksandrov and K. M. Neyman, *J. Phys. Chem. C*, 2015, **119**, 5180–5186.
54 T. L. Tan, L. Wang, D. D. Johnson and K. Bai, *J. Phys. Chem. C*, 2013, **117**, 22696–22704.
55 S. Gudmundsdóttir, E. Skúlason, K.-J. Weststrate, L. Juulink and H. Jónsson, *Phys. Chem. Chem. Phys.*, 2013, **15**, 6323–6332.
56 L. Yan, Y. Sun, Y. Yamamoto, S. Kasamatsu, I. Hamada and O. Sugino, *J. Chem. Phys.*, 2018, **149**, 164702.
57 N. B. Arboleda Jr, H. Kasai, W. A. Diño and H. Nakanishi, *Jpn. J. Appl. Phys.*, 2007, **46**, 4233–4237.
58 Y. Dong, M. Ebrahimi, A. Tillekaratne and F. Zaera, *J. Phys. Chem. Lett.*, 2016, **7**, 2439–2443.
59 Y. Li and R. T. Yang, *J. Am. Chem. Soc.*, 2006, **128**, 8136–8137.
60 C.-S. Tsao, Y.-R. Tzeng, C.-Y. Wang, H.-H. Tseng, T.-Y. Chung, H.-C. Wu, T. Yamamoto, K. Kaneko and S.-H. Chen, *J. Phys. Chem. Lett.*, 2010, **1**, 1060–1063.
61 Z. G. Bajestani, A. Yürüm and Y. Yürüm, *Int. J. Hydrogen Energy*, 2016, **41**, 9810–9818.